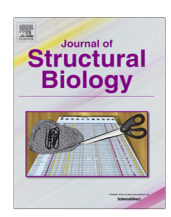
ELSEVIER

Contents lists available at ScienceDirect

### Journal of Structural Biology

journal homepage: www.elsevier.com/locate/yjsbi



## Molecular basis for the formation of ribonucleoprotein complex of Crimean-Congo hemorrhagic fever virus



Xiaojing Wang <sup>a,1</sup>, Baobin Li <sup>b,g,1</sup>, Yu Guo <sup>c,d</sup>, Shu Shen <sup>e</sup>, Liang Zhao <sup>a</sup>, Peisheng Zhang <sup>b</sup>, Yuna Sun <sup>d</sup>, Sen-Fang Sui <sup>a,\*</sup>, Fei Deng <sup>e,\*</sup>, Zhiyong Lou <sup>b,c,f,\*</sup>

- a State Key Laboratory of Biomembrane, Beijing Advanced Innovation Center for Structural Biology, School of Life Sciences, Tsinghua University, Beijing 100084, China
- <sup>b</sup> School of Medicine and MOE Laboratory of Protein Science, Tsinghua University, Beijing 100084, China
- <sup>c</sup>College of Pharmacy and State Key Laboratory of Medicinal Chemical Biology, Nankai University, Tianjin 300071, China
- d National Laboratory of Macromolecules, Institute of Biophysics, Chinese Academy of Science, Beijing 100101, China
- <sup>e</sup> State Key Laboratory of Virology, Wuhan Institute of Virology, Chinese Academy of Sciences, Wuhan 430071, China
- f State Key Laboratory of Biotherapy and Collaborative Innovation Center of Biotherapy, West China Hospital, Sichuan University, Chengdu 610041, China
- g School of Pharmacy, University of Wisconsin–Madison, Madison, WI 53705, USA

#### ARTICLE INFO

# Article history: Received 27 July 2016 Received in revised form 20 September 2016 Accepted 20 September 2016 Available online 22 September 2016

Keywords: CCHFV Nucleocapsid protein Oligomer Architecture

#### ABSTRACT

Negative-sense single-strand RNA (-ssRNA) viruses comprise a large family of pathogens that cause severe human infectious diseases. All -ssRNA viruses encode a nucleocapsid protein (NP) to encapsidate the viral genome, which, together with polymerase, forms a ribonucleoprotein complex (RNP) that is packaged into virions and acts as the template for viral replication and transcription. In our previous work, we solved the monomeric structure of NP encoded by Crimean-Congo hemorrhagic fever virus (CCHFV), which belongs to the Nairovirus genus within the Bunyaviridae family, and revealed its unusual endonuclease activity. However, the mechanism of CCHFV RNP formation remains unclear, due to the difficulty in reconstructing the oligomeric CCHFV NP-RNA complex. Here, we identified and isolated the oligomeric CCHFV NP-RNA complex that formed in expression cells. Sequencing of RNA extracted from the complex revealed sequence specificity and suggested a potential encapsidation signal facilitating the association between NP and viral genome. A cryo-EM reconstruction revealed the ring-shaped architecture of the CCHFV NP-RNA oligomer, thus defining the interaction between the head and stalk domains that results in NP multimerization. This structure also suggested a modified gating mechanism for viral genome encapsidation, in which both the head and stalk domains participate in RNA binding. This work provides insight into the distinct mechanism underlying CCHFV RNP formation compared to other ssRNA viruses.

© 2016 Elsevier Inc. All rights reserved.

#### 1. Introduction

Negative-sense single-stranded RNA (-ssRNA) viruses comprise the Mononegavirales order (*Rhabodviridae*, *Paramyxoviridae*, *Bor-naviridae* and *Filoviridae* families) and three individual families (*Arenaviridae*, *Bunyaviridae* and *Orthomyxoviridae*), including numerous pathogens, e.g., Ebola virus, influenza virus, Lassa fever virus (LASV), and Crimean-Congo hemorrhagic fever virus (CCHFV), among others, which cause severe infectious diseases in humans. All -ssRNA viruses encode a nucleocapsid protein (NP) that encapsidates RNA and, with viral polymerase, forms a ribonucleoprotein complex (RNP) that is packaged into virions to serve as a template for RNA synthesis (Elliott, 2014; Lou et al., 2014; Ruigrok et al., 2011; Sun et al., 2012; Zhou et al., 2013a).

Bunyaviruses constitute the largest -ssRNA virus family and are subdivided into the *Orthobunyavirus*, *Hantavirus*, *Nairovirus*, *Phlebovirus*, and *Tospovirus* genera (Guo et al., 2012). The genomes of all bunyaviruses include a large (L), middle (M), and small (S) segment (Eifan and Elliott, 2009; Elliott, 1990); among these, the L segment encodes an RNA-dependent RNA polymerase (RdRp), the M segment encodes a glycoprotein precursor (Gn and Gc), and the S segment encodes the NP protein. Several *Bunyaviridae* 

Abbreviations: CCHFV, Crimean-Congo hemorrhagic fever virus.

<sup>\*</sup> Corresponding authors at: School of Medicine and MOE Laboratory of Protein Science, Tsinghua University, Beijing 100084, China (Z. Lou).

*E-mail addresses*: suisf@mail.tsinghua.edu.cn (S.-F. Sui), df@wh.iov.cn (F. Deng), louzy@mail.tsinghua.edu.cn (Z. Lou).

<sup>&</sup>lt;sup>1</sup> These authors contribute equally to this work.

members also possess a nonstructural protein (NSs and/or NSm) that employs an ambisense coding strategy for the S and M segments (Jiao et al., 2011).

Similar to other -ssRNA viruses, bunyaviruses facilitate the encapsidation of their genome by viral NP encoded by the S segment; however, their NPs demonstrate significant variations (Lou et al., 2014; Sun et al., 2012; Zhou et al., 2013a). The NPs of Rift Valley fever virus (RVFV), severe fever with thrombocytopenia syndrome virus (SFTSV) and Toscana virus, which are members of the *Phlebovirus* genus, undergo novel protein folding and facilitate oligomerization through their N-terminal arms (Jiao et al., 2013; Olal et al., 2014; Raymond et al., 2010, 2012; Reguera et al., 2013; Zhou et al., 2013b). Analysis of the NP-RNA complex structures of Bunyamwera virus (BUNV) (Li et al., 2013a), Leanyer virus (LEAV) (Niu et al., 2013), La Crosse orthobunyavirus (LACV) (Reguera et al., 2013), and Schmallenberg virus (SBV) (Dong et al., 2013b) revealed N- and C-terminal extensions that mediate the inter-protomer interactions of these orthobunyaviral NPs.

CCHFV, a representative member of the Nairovirus genus, encodes an NP with the largest molecular weight in the Bunyaviridae family (Guu et al., 2012; Li et al., 2013a). We previously determined the crystal structure of CCHFV (strain YL04057) NP in a monomeric form, which presents a racket-shaped structure with head and stalk domains (Guo et al., 2012). Although the head domain of CCHFV NP shares high structural similarity to the Nterminal domain of LASV NP, it exhibits unusual metaldependent DNA-specific endonuclease activity (Guo et al., 2012). Subsequently, Carter et al. reported the structure of NP from the CCHFV strain Baghdad-12 and revealed significant transposition of the stalk domain through a 180° rotation and a 40 Å translation compared to the NP from strain YL04057, indicating structural flexibility to switch between alternative NP conformations during RNA binding or oligomerization (Carter et al., 2012). Furthermore, Wang et al. studied the structure of CCHFV (strain IbAr10200) NP pre-treated with poly(rU) and revealed another conformational shift on the stalk domain (Wang et al., 2012). Although a headto-tail interaction of the stalk domain with the base of the head domain of the adjacent subunit was proposed to stabilize the super-helical organization of the oligomeric form of CCHFV NP (strain IbAr10200) based on the crystal structure of poly(rU)pretreated multimers, poly(rU) is not found in the structure and a true oligomerization state was not experimentally observed (Wang et al., 2012). Therefore, it is important to address two key questions regarding CCHFV RNP formation that remain unclear due to failure in reconstructing the oligomeric CCHFV NP-RNA complex: 1) how CCHFV NP oligomerizes to form high-ordered RNP and 2) how CCHFV NP encapsidates and protects the viral genome. These questions prompted us to perform further structural and functional investigations.

#### 2. Materials and methods

#### 2.1. Purification of the CCHFV NP-RNA Complex

The full-length CCHFV NP (strain YL04057) gene was cloned into the pGEX-6p-1 (GE Healthcare) expression vector (Novagen) using *Nde*I and *Xho*I restriction enzyme sites. The plasmid was transformed into *E. coli* strain BL21 (DE3) for GST fusion protein overexpression, and the transformed cells were cultured at 37 °C in LB media containing 100 mg/I ampicillin. After the OD $_{600}$  reached 0.6, the culture was cooled to 16 °C, and IPTG was added to a final concentration of 0.3 mM to induce the expression of recombinant protein. After overnight induction, the cells were harvested by centrifugation. The pellets were then resuspended in lysis buffer containing 20 mM Tris (pH 8.0) and 150 mM NaCl, fol-

lowed by homogenization using an ultra-high-pressure cell disrupter (JNBIO, Guangzhou, China) at  $4\,^{\circ}$ C. The insoluble material was removed by centrifugation at  $25,000\times g$  for 30 min at  $4\,^{\circ}$ C. The fusion protein was first purified by GST column chromatography pre-equilibrated with lysis buffer. Then, the column was washed five times in the same buffer, and the GST tag was removed via digestion with PreScission protease (GE Healthcare) overnight at  $4\,^{\circ}$ C. The target protein was eluted, and the fractions were further purified on a Superdex-200 gel filtration column (GE Healthcare). The peak-2 fractions were collected and further purified through a Superdex-200 gel filtration column again to isolate the CCHFV NP-RNA complex.

#### 2.2. RNA extraction and analysis

Total RNA was harvested from the CCHFV NP-RNA complex via sequential extractions with equal volumes of a phenol and chloroform mixture, followed by ethanol precipitation and RNA resuspension, as previously reported (Mohl and Barr, 2009). The quality and quantity of the RNA were checked using a Nanodrop. 100 ng RNA were used for library preparation. Illumina pairedend index library construction was carried out according to the manufacturer's recommendations (NEBNext® Ultra™RNA Library Prep Kit for Illumina<sup>®</sup>). Briefly, first-strand cDNA was synthesized using ProtoScript II Reverse Transcriptase, and second-strand cDNA was synthesized using Second Strand Synthesis Enzyme Mix. Double-stranded cDNA was purified using the AxyPrep Mag PCR Clean-up Kit (Axygen) and then treated with End Prep Enzyme Mix for end repair, 5' phosphorylation and the addition of "A" bases to the ends of double-stranded DNA fragments in one reaction, followed by ligation to adaptors with a "T" base overhang. Adaptor-ligated DNA fragments of  $\sim$ 400 bp (with an approximate insert size of 250 bp) were selected and recovered using the Axy-Prep Mag PCR Clean-up Kit (Axygen). Index sequences were added to adapter-modified DNA fragments during the PCR enrichment step. Then, libraries with different indexes were loaded on an Illumina HiSeq instrument according to the manufacturer's instructions (Illumina, San Diego, CA, USA) (Guo et al., 2013). Sequencing was carried out using a 2 × 100 paired-end (PE) configuration; image analysis, and base calling was carried out using the Illumina pipeline, specifically HiSeq Control Software (HCS) + OLB + GAPipeline-1.6 (Illumina). The sequences were processed and analyzed by GENEWIZ using Trimmomatic (version 0.30) and PerlScript.

#### 2.3. Purification of native CCHFV RNPs

Virus particles were concentrated and purified as previously described, with modifications (Ariza et al., 2013). Vero cells were infected with CCHFV at a multiplicity of infection (MOI) of 0.01. Supernatants were harvested at 7 d post-infection (p.i.), clarified at 4500 rpm for 5 min at 4 °C and further filtered through a 0.45μM filter to remove cell debris. The filtered supernatants were mixed with 0.5 M NaCl and 10% (w/v) PEG-6000 (Sigma), then stirred on ice for 20 min and left overnight at 4 °C. Viruses were precipitated via centrifugation at 3000 rpm for 30 min at 4 °C. The pellets were resuspended in cold TEN buffer (100 mM NaCl, 1 mM EDTA, 0.01 M Tris-HCl, pH 7.4) and loaded on top of a 5-25% continuous Optiprep iodixanol density gradient (Sigma). The gradient was prepared by layering (from bottom to top, in an 0.8 ml volume) 25%, 20%, 15%, 10% and 5% (v/v) Optiprep iodixanol density gradient dissolved in TEN buffer with protease inhibitor (Roche), with incubation overnight at 4 °C. Virus preparations were centrifuged for 1.5 h at 28,000×g. Fractions of 500 µl were collected from the bottom of the gradient and treated with 1% (w/v) saponin (Sigma) dissolved in TES buffer (0.05 M Tris-HCl, pH 8.2, 1 mM EDTA and 0.15 M NaCl) to release RNPs as previously described (Arstila, 1974).

#### 2.4. Negative-stain electron microscopy

Grids for negative-stain EM were prepared using a conventional method (Li et al., 2013a). 5  $\mu$ l purified CCHFV NP protein sample was applied to glow-discharged EM grids covered with a thin layer of carbon film and stained with 2% (w/v) uranyl acetate. Images were taken using an FEI Tecnai Spirit BioTWIN D1266 electron microscope and recorded at a magnification of 68,000× using a 4 k × 4 k charge-coupled device camera, corresponding to a pixel size of 1.6 Å per pixel on the specimen. Tilt-pair images for random conical tilt 3D reconstruction were manually recorded. For 2D analysis, 5730 particles were interactively selected from 150 images. Reference-free 2D classification was carried out by RELION (Scheres, 2012).

#### 2.5. Cryo-electron microscopy

4 ul aliquots at 1.2 mg/ml were loaded onto glow-discharged grids. Grids were blotted for 3 s and frozen by plunging into liquid ethane cooled by liquid nitrogen using an FEI Vitrobot IV. Grids were checked using an FEI Tecnai Spirit BioTWIN D1266 operated under low-dose conditions to ensure that the thickness of the ice was appropriate for data collection and there was no obvious preferred orientation observed. Grids were then transferred to a Titan Krios operated at 300 kV for data collection. Images were recorded on a Gatan K2 Summit direct electron detector operated in superresolution counting mode following an established dose fractionation data acquisition protocol (Li et al., 2013c). Images were recorded at a nominal magnification of 22,500×, corresponding to a calibrated super-resolution pixel size of 0.66 Å on the specimen. The dose rate on the detector was set at  $\sim$ 8.2 counts. The total exposure time was 8 s. Dose-fractionated images were recorded using the semi-automated acquisition program UCSF Image4 (written by Xueming Li). Defocus values ranged from -2to 3.5 µm.

Super-resolution counting images were  $2 \times 2$  binned for motion correction, resulting in a pixel size of 1.32 Å. Motion-corrected frames were summed to a single micrograph for subsequent processing. Defocus values were determined for each micrograph using CTFFIND3 (Mindell et al., 2003). A semi-automated procedure was used to pick particles. The particles were rescaled 2 times, resulting in a pixel size of 2.64 Å for further image processing. 2D classification and 3D classification were performed using RELION followed by 3D refinement. The negative-stain model was used for 3D classification as an initial model. The 3D refinement containing 10,713 particles was imposed C5 symmetry, using gold-standard FSC calculations to avoid overfitting, and the reported resolution of 9.38 Å was based on the FSC = 0.143 criterion (Supplementary Fig. S3) (Scheres and Chen, 2012). The Bfactor was automatically determined by RELION postprocess procedure.

#### 2.6. Model building

Model building of the isolated head and stalk domains of the CCHFV NP monomer (PDB code: 3U3I) was performed using UCSF Chimera (Pettersen et al., 2004) for rigid body fitting. The docking also confirmed the handedness of the density map. COOT (Emsley et al., 2010) was then used for model optimization.

#### 2.7. Endonuclease activity assay

A DNA cleavage assay was performed as previously reported. Briefly,  $0.3~\mu M$  monomeric CCHFV NP or fresh purified CCHFV NP-RNA complex was incubated with  $100~ng/\mu l$  179-nt ssDNA at 37 °C in a final volume of  $10~\mu l$ . The reaction buffer was 20~mM HEPES, 200~mM NaCl, and 1~mM manganese chloride at pH 7.0. Reactions were stopped via the addition of EDTA to a final concentration of 10~mM, and reaction products were loaded on a 1.5% agarose gel and stained with ethidium bromide.

#### 2.8. CCHFV mini replicon assay

Briefly, a reporter plasmid (pRF-T7-S-hGluc) was generated by replacing the NP open reading frame (ORF) with the Gaussia Luciferase gene (Promega), followed by cloning into the modified vector pRF-T7; then, the T7 promoter and HDV ribozyme/T7 terminator were inserted into pRF42 (Flick and Whitehouse, 2005) to produce viral sense RNAs. The wild type or mutated NP gene was cloned into pcDNA3.1(+) as previously described (Li et al., 2013b). To construct the CCHFV L ORF expression plasmid, six fragments (L1, 1-1771 nt; L2, 1710-3256 nt; L3, 3197-5956 nt; L4, 5897-9054 nt; and L5, 8995-11838 nt fusion with a Flag tag) of the L ORF were amplified using CCHFV RNA (strain YL04057) as a template with the primers listed in Table S2. The CMV promoter and BGH poly A sequences were amplified from pcDNA3.1(+) (Invitrogen). Each fragment shares regions of  $\sim$ 60 bp with the neighboring fragments at both the 5' and 3' ends. These fragments were cloned into the pT-Easy plasmid (Promega), sequenced and then digested by BsmBI or BsaI for use in the following process. 50 ng of the pGF plasmid (a shuttle plasmid in E. coli and yeast, unpublished data) were digested with EcoRI and BamHI, and 100 ng of each digested fragment was incubated with 200 µl of yeast spheroplasts for 10 min. Then, 800 ul of PEG 8000 solution was added and incubated for 10 min at room temperature. The spheroplasts were pelleted and recovered in rich medium for 40 min, then transferred to selective medium in the absence of histidine as previously described (Kouprina and Larionov, 2008). Positive clones containing the Flag-tagged L ORF flanked by the CMV promoter and BGH poly A (pGF-CMV-LFlag) were identified using PCR. BSR/T7 cells were seeded in 48-well plates at a density of  $3 \times 10^4$  cells/well. The cells in each well were transfected with 350 ng of pGF-CMV-LFlag, 150 ng of WT pcDNA-NP or mutants, and 30 ng of pRF-T7-S-hGluc. At 48 h p.t., the supernatants were harvested to measure luciferase activity with a Gaussia Luciferase Assay Kit (New England Biolabs) on a Synergy 4 microplate reader (BioTek). Luciferase activity was expressed as a percentage of the wt-NP control.

#### 3. Results

#### 3.1. Identification and isolation of the CCHFV NP oligomer in solution

An understanding of the molecular mechanism of viral RNP formation is dependent on the successful acquisition of homogeneous viral NP-RNA complexes *in vitro*, which is primarily achieved using two methods: 1) expression of the recombinant NP and purification of the NP-RNA complex that forms in expression cells (Albertini et al., 2006; Green et al., 2006; Hastie et al., 2011b; Li et al., 2013a; Niu et al., 2013; Tawar et al., 2009), or 2) incubation of NP with nucleic acid *in vitro* and reconstruction of the NP-RNA complex (Jiao et al., 2013; Raymond et al., 2012).

In our previous study, we expressed the full-length CCHFV NP in *Escherichia coli* (*E. coli*) and revealed that it predominantly exists in the form of monomers or inhomogeneous higher-order oligomers

with large molecular weights under physiological conditions (Guo et al., 2012). We then performed biochemical experiments to identify the potential oligomers of CCHFV NP. Investigation of CCHFV (strain IbAr10200) NP suggested the induction of CCHFV NP multimerization via pre-treatment with poly(rU) (Wang et al., 2012). We thus hypothesized that we would obtain the oligomeric CCHFV NP-RNA complex by supplementing the monomeric CCHFV NP with additional random nucleic acids. However, all attempts to utilize variable nucleic acids or manipulate incubation conditions ultimately failed, suggesting an essential RNA sequence or structural specificity that is essential for association with CCHFV NP.

We then performed size exclusion chromatography (SEC) to verify the recombinant CCHFV NP expressed in E. coli. Two major peaks, peak-1 and peak-4, were identified. Peak-4 eluted at 15 ml in Superdex-200 column and represented the monomeric CCHFV NP (Guo et al., 2012), whereas peak-1 in exclusion volume consisted of inhomogeneous high-ordered target protein contaminated by other proteins (Fig. 1A and B). In addition to peak-1 and peak-4, there were two additional minor peaks, peak-2 and peak-3, which were previously not addressed (Fig. 1A). According to SDS-PAGE analysis, peak-2 consisted of highly pure CCHFV NP, whereas peak-3 demonstrated heavy protein contamination (Fig. 1B). However, the amount of peak-2 was extremely small, i.e., less than 1% of the total amount of expressed CCHFV NP protein, making further analysis difficult. We cultured over 500 L of E. coli to isolate, enrich, and re-purify the peak-2 fraction using SEC. According to the gel filtration results, the peak-2 fraction presented a single peak with an elution volume of 11.6 ml, indicating a stable oligomerization (Fig. 1C and D).

Peak–4 contained the CCHFV NP monomer without nucleic acid, and the optical density (OD) ratio of 260 nm to 280 nm (OD $_{260}$ /OD $_{280}$ ) was 0.6 (Fig. 1A), demonstrating the absence of nucleic acid in the monomeric structure (Guo et al., 2012). Conversely, the ratio of OD $_{260}$ /OD $_{280}$  for peak–2 was approximately 1.3 (Fig. 1C), suggesting this sample bound with nucleic acid obtained from expression cells. We therefore speculated that peak–2 represents the CCHFV NP–RNA complex in its oligomeric state.

# 3.2. Electron microscopy (EM) of the recombinant CCHFV NP-RNA oligomer

To verify the multimerization state of the CCHFV NP-RNA complex in solution, we first visualized the peak-2 sample using negative-stain electron microscopy (EM) (Supplementary Fig. S1A). The CCHFV NP oligomer formed four types of ring-shaped oligomers with diameters ranging from 120 Å to 220 Å. These particles predominantly consisted of pentamers (70%), followed by hexamers (23%), tetramers (4%) and heptamers (3%) (Supplementary Fig. S1B). Moreover, the left and right regions of the head domain in addition to the stalk domain of the CCHFV NP monomer were clearly observed in an enlarged EM image (Supplementary Fig. S1A). These results confirmed our hypothesis that the peak-2 fraction contained CCHFV NP-RNA oligomers and revealed that these oligomers presented a ring-shaped architecture.

#### 3.3. Analysis of RNA bound to the CCHFV NP-RNA complex

In previous studies, recombinant NPs, which can form ring-shaped NP-RNA complexes in expression cells, bound non-specific RNA randomly acquired from host cells (Albertini et al., 2006; Green et al., 2006; Qing et al., 2014; Tawar et al., 2009). Structural and biochemical studies have consistently suggested no RNA sequence specificities of orthobunyavirus NPs (Ariza et al., 2013; Dong et al., 2013a; Li et al., 2013a; Niu et al., 2013; Reguera et al., 2013). In all previously reported NP-RNA structures, the oligomeric form has been present in a dominant state during

the expression and purification of the recombinant NP-RNA complex. In sharp contrast, oligomeric CCHFV NP-RNA complexes occupied less than 1% of the total amount of expressed CCHFV NP in our study (Fig. 1A). We therefore hypothesized that RNA present in the CCHFV NP-RNA complexes possessed a specific sequence or structure to facilitate their association with NP. Moreover, because the generally accepted unidirectional encapsidation model assumes that NP first binds to an encapsidation signal in an RNA string and then enwraps the RNA in the 5′ to 3′ direction, we also hypothesized the presence of a potential encapsidation signal in the bound RNA.

To test this hypothesis, we extracted RNA from the purified CCHFV NP-RNA complex and performed cDNAs transcription following a previously reported protocol (Mohl and Barr, 2009). We generated standard Illumina sequencing libraries and performed sequencing using an Illumina HiSeq 2000 instrument according to the  $2 \times 100$ -bp paired-end read sequencing protocol. We obtained 130,000 reads and undertook quality control analysis, resulting in 42,699 reads. A total of 12.1% of the sequences were present in cloning vectors, 82.4% matched the E. coli genome, and 5.5% exactly matched the CCHFV S segment. 28 sequences had over 100 readout counts (Table S1). The sequenced RNAs ranged in length from 76 to 102 nt, and the most abundant group possessed lengths of 76–79 nt (13 sequences out of 28 total sequences). Given our hypothesis that each NP protomer binds an RNA of equal length and because pentamers/hexamers are the dominant oligomeric states, we proposed the binding of 13–15 bases of the CCHFV NP protomer during RNA encapsidation. No sequenced RNAs demonstrated lengths over 150 nt, suggesting the absence of a high-ordered CCHFV NP-RNA complex in the purified sample.

The top 28 sequences were analyzed, and all possessed a stem-loop secondary structure. Seq-3, -16 and -17, which mapped to the CCHFV S segment 5' cRNA (R1 region) (Table S1), formed the stem-loop secondary structure (Supplementary Fig. S2A). Moreover, a strictly conserved region of the Seq-1, -2 and -4 RNAs from *E. coli*, which demonstrated a remarkably high readout count (a total of 9191 readout counts) within all sequenced-out RNAs (42,669 readout counts), mapped strongly in both the 5' and 3' ends of the CCHFV S segment (Supplementary Fig. S2B). Based on these results, the secondary structure may act as an encapsidation signal at the ends of the CCHFV genome, similar to that observed in other bunyaviruses (Mir et al., 2006; Osborne and Elliott, 2000).

#### 3.4. Organization of the CCHFV NP-RNA oligomer

Because the predominant state of the CCHFV NP-RNA complex was a pentamer form, we reconstructed the three-dimensional (3D) structure of the pentamer at a resolution of 9.4 Å using cryo-EM (Fig. 2A; Supplementary Fig. S3). Based on the 3D reconstruction, the CCHFV NP-RNA complex exhibited a ring-shaped stalk-to-head architecture in a clockwise direction (Fig. 2). The orientations of the head and stalk domains of CCHFV NP demonstrated significant changes (Carter et al., 2012; Wang et al., 2012). Therefore, the head (M1-I180 and G301-I482) and stalk domains (R195-Q300) derived from the crystal structure of the CCHFV NP monomer (PDB code: 3U3I) (Guo et al., 2012) were separately fit into the EM map with the aid of automated docking procedures employing structural and biological restraints (Pettersen et al., 2004).

Although the modest resolution map did not permit atomic interpretation, the protomer arrangement and NP domains were localized within the pentamer (Fig. 2A). Inter-protomer interactions were mainly attributable to the right portion of the head domain of one NP protomer and the bottom region of the stalk domain of an adjacent NP protomer on the left side. Compared to the monomeric structure of CCHFV NP, the orientation of the stalk

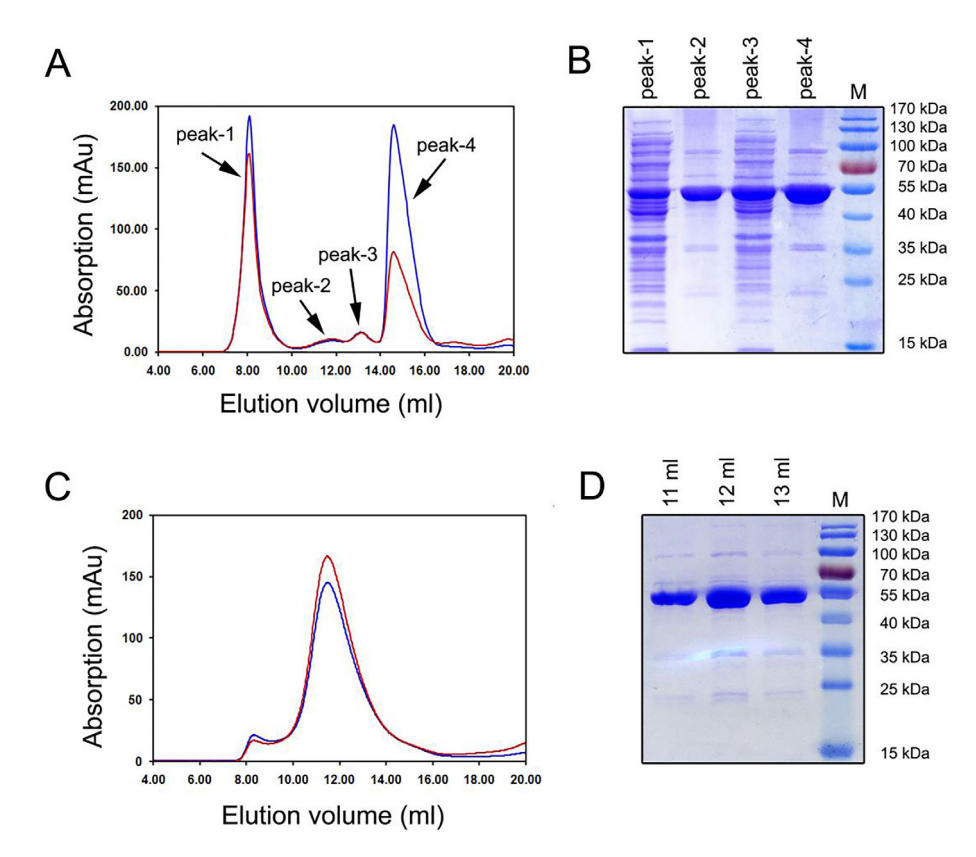


**Fig. 1.** Size exclusion chromatography (SEC) and SDS-PAGE analysis. (A) Full-length CCHFV NP expressed in *E. coli* (0.2 mg) was injected into a Superdex-200 HR 10/30 column. The retention volumes for peaks-1, -2, -3 and -4 were 8 ml, 11.6 ml, 13.2 ml and 15 ml, respectively. The absorbances at 260 and 280 nm are indicated in red and blue, respectively. (B) SDS-PAGE analysis of four peaks. Because the amounts of peak-2 and peak-3 were extremely small, these two fractions were concentrated before they were loaded onto the SDS-PAGE gel. All samples were loaded onto a 15% SDS-PAGE gel containing approximate 10 μg of protein. A standard protein marker is shown in the right lane. (C) The fractions for peak-2 were enriched and re-loaded into a Superdex-200 HR 10/30 column, and the retention volume for the single peak of peak-2 was 11.6 ml. (D) Fractions representing elution volumes of 11, 12 and 13 ml were loaded onto a 15% SDS-PAGE gel. A standard protein marker is shown in the right lane.

domain of each protomer involves a rotation of approximately 120° at the end (residue A300) (Fig. 2B). The relative orientations of the head and stalk domains in CCHFV NP oligomer are also distinct from the NP structures of CCHFV strain Baghdad-12 (PDB code: 4AKL) and strain IbAr10200 with (PDB code: 4AQF) or without poly(rU) pre-treatment (PDB code: 4AQG) (Supplementary Fig. S4) (Wang et al., 2012).

#### 3.5. Inter-protomer interactions

The assembled RNPs comprise a large number of copies of NP bound to genomic RNA and one NP protomer interacts with adjacent NP molecules to maintain the oligomeric architecture (Green et al., 2006). Cryo-EM reconstruction of the CCHFV NP-RNA complex allowed us to identify two regions accounting for inter-protomer interactions (Fig. 3).

One region was present in the head domain and predominantly contained the residues L26, V27, T29, F30, F36, C37, E38, S39, and F73 (Fig. 3B). The second region was located at the remote end of the stalk domain and contained the residues K265, D266, E267, V268, D269, R270, and S272 (Fig. 3C). The stalk domain of one NP protomer interacted with the head domain of an adjacent NP protomer on the right and formed a ring-shaped stalk-to-head architecture in a clockwise direction.

The remote end of the stalk domain, which is a key interprotomer region, contained a previously identified host caspase-3 proteolytic cleavage site with the following protein sequence: DEVD (Karlberg et al., 2011). Because this site participates in the

formation of the CCHFV NP oligomer, oligomerization potentially prevents the cleavage of CCHFV NP by caspase-3, which was demonstrated in a previous study (Wang et al., 2012). Participation of the end of the stalk domain in CCHFV NP inter-protomer contact was also indicated by the structure of CCHFV NP strain IbAr10200 (Wang et al., 2012); however, the interacting region in the head domain was completely different compared to those of the CCHFV NP strains IbAr10200 and Baghdad-12 (Carter et al., 2012) (Supplementary Fig. S5). Therefore, we hypothesized that replacement of the residues of the head domain, which is likely located at the dimer interface as indicated by the structure of CCHFV NP strain Baghdad-12 and specifically contains E108, E112, K114, K354, and others, would negatively impact CCHFV proliferation (Carter et al., 2012) and other biological processes during NP functions.

To further verify the role of these residues at the inter-protomer interface in NP oligomerization, we performed alanine substitutions and evaluated whether these mutations disrupted interprotomer binding using pull-down assays (Fig. 3D and E). Four substitutions, G25A, L26A, F36A, and V268A, resulted in the greatest attenuation (less than 30% compared with wt-NP) of interprotomer binding, indicating the critical roles of these residues in inter-protomer interactions. Conversely, the replacement of V27, F30, C37 and S272 with alanine resulted in the retention of over 75% inter-protomer binding ability. Other mutations, including T29A, K265A, D266A, E267A and R270A, reduced NP-NP binding by 50%. All of these results supported our EM reconstruction in which both the head and stalk domains are responsible for CCHFV RNP formation.

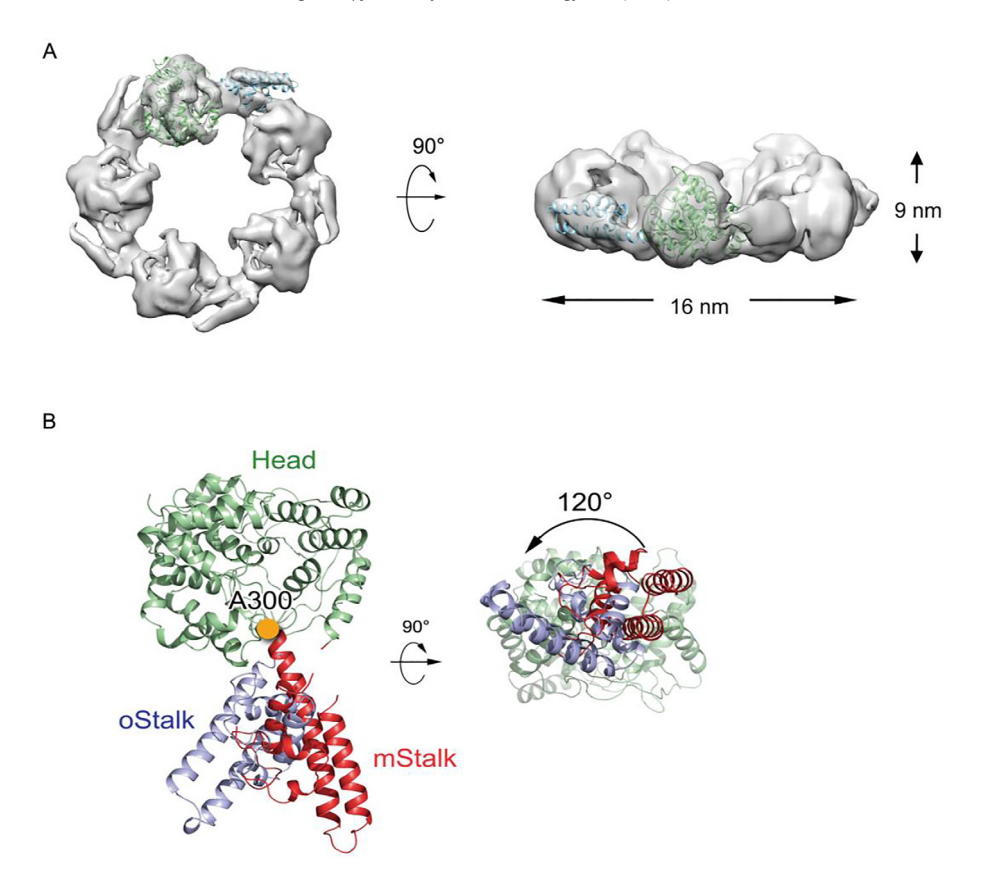


Fig. 2. Organization of the CCHFV NP oligomer. (A) Three-dimensional reconstruction of the CCHFV NP pentamer with the crystal structure (PDB code: 3U3I) (Guo et al., 2012) of the head and stalk domains individually docked into the map. The head and stalk domains of each protomer are colored in pale green and light blue, respectively. (B) Comparison of the orientations of the head and stalk domains in the monomeric and oligomeric states from two perpendicular views. The monomeric structure is represented by the structure of CCHFV (strain YL04057) NP (PDB code: 3U3I) (Guo et al., 2012). The head domains of the two structures are colored in pale green, while the stalk domains in the monomer (mStalk) and oligomer (oStalk) are shown in red and light blue.

To further verify the impact of these residues on CCHFV NP oligomerization, we next tested the effects of their substitution in the previously reported CCHFV mini replicon system, in which reporter gene expression depends on the ability of NP to bind RNA and multimerize to form RNPs (Bergeron et al., 2012: Carter et al., 2012) (Fig. 3F). Based on the expression levels of the reporter gene, L26A and F36A demonstrated the greatest impact on replicon activity, which is consistent with the results of the pull-down assay. G25A mutation substantially decreased NP-NP interactions but resulted in only modest attenuation of replicon activity, indicating an additional complementary mechanism for these two sites in native CCHFV RNP. The same observations were also made for the K265 and D266 positions; alanine substitution resulted in  ${\sim}50\%$  attenuation of NP-NP interactions but exerted only minor effects on replicon activity. Conversely, alanine substitution of E267, V268, and R270 consistently impacted inter-protomer interactions and replicon activity (Fig. 3F). These results reveal the complexity of the biological function of the remote end of the CCHFV NP stalk domain.

#### 3.6. Channel for RNA encapsidation

The OD<sub>260</sub>/OD<sub>280</sub> ratio of the purified peak-2 fraction was approximately 1.3, indicating that the oligomeric CCHFV NP binds RNA obtained from host cells (Fig. 1C). Based on the top view of the pentamer, the NP orientation directs the proposed NP-RNA binding channel into the inner side of the ring-shaped oligomer (Fig. 4A). The deep groove within the head domain, which is the active site of endonuclease activity, and residues from the stalk domain com-

prise a positively-charged region found in all NP protomers that forms a consecutive RNA binding channel along the inner perimeter of the pentameric ring. These residues include R45, K72, S149, H197, K222, R225, K237, Q303, K336, R339, K342, K343, K345, R372, and K462 (Fig. 4B). In the oligomer, the chain-like viral genome passes through the deep groove of the head domain, contacts the stalk domain and extends to the head domain of an adjacent NP protomer in a clockwise direction.

In our previous study, the CCHFV NP monomer degraded both double-strand (ds) and single-strand (ss) DNA with metal ion dependence but did not cleave RNA, dsRNA or ssRNA (Guo et al., 2012). Furthermore, the deep groove in the head domain was the active site of the endonuclease activity exhibited by the CCHFV NP monomer. We thus hypothesized that the oligomeric CCHFV NP-RNA complex would not retain this endonuclease activity because the active site in the head domain was occupied by RNA molecules. We therefore evaluated the endonuclease activity of the CCHFV NP-RNA oligomer. Consistent with our hypothesis, the CCHFV NP-RNA complex in the peak-2 fraction did not degrade a DNA probe, in contrast to the CCHFV NP monomer (Fig. 4C).

#### 3.7. Visualization of authentic CCHFV RNP

In previous studies, native RNPs extracted from bunyavirus virions exhibited distinct architectures: either a flexible structure with a monomer-sized NP-RNA complex as the building block or a structure possessing helical characteristics, potentially resulting from a different protocol for purification and EM staining (Ariza et al., 2013; Li et al., 2013a; Niu et al., 2013; Raymond et al., 2010;

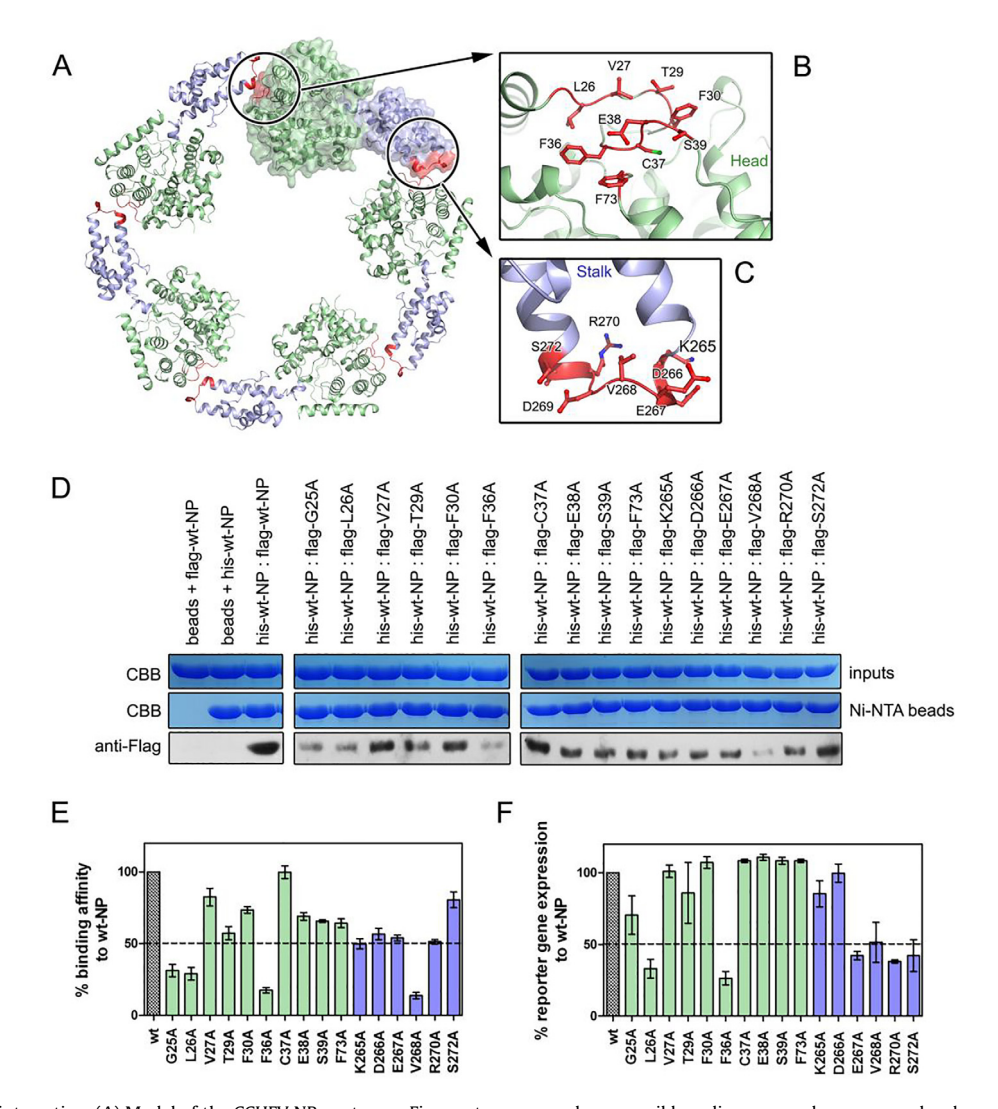


Fig. 3. Inter-protomer interaction. (A) Model of the CCHFV NP pentamer. Five protomers are shown as ribbon diagrams and one as a molecular surface. The head and stalk domains of each protomer are colored in pale green and light blue, respectively, and the residues located at the inter-protomer interface are colored in red. Residues for interprotomer interaction at the head (B) and stalk (C) domains are highlighted in the enlarged representations. (D) Pulldown assay to test the impact of mutations on the NP-NP interaction. The results were quantified using the ImageJ software and are shown in (E). (F) BSR/T7 cells were transfected with pGF-CMV-LFlag, the reporter plasmid pRF-T7-S-hGluc and the wt-NP expression plasmid pcDNA-NP or each of the mutants with substitutions at the residues found at the inter-protomer interface. Luciferase activity was measured at 48 h post-transfection. Each experiment was performed with three replicates, and error bars indicate standard deviations.

Reguera et al., 2013). Therefore, we extracted natural RNP from CCHFV virions and performed negative-stain EM to observe the architecture of the native CCHFV RNP (Fig. 5).

CCHFV virions released by infected Vero cells were purified and treated with 1% (w/v) saponin (Arstila, 1974) to open the viruses and release the natural RNPs. These RNPs were further purified but were not disrupted or modified by isolation procedures. The majority of natural RNPs exhibited a relaxed architecture with a width of approximate 50 Å (Fig. 5A). Interestingly, a few native RNPs displayed apparent helical characteristics with an approximate diameter of 120 Å (Fig. 5B), which is consistent with the smallest diameter of the recombinant CCHFV NP-RNA oligomer. Based on these results, the monomer-sized CCHFV NP-RNA complex is the building block of the relaxed CCHFV RNP, and these RNPs further assume a helical architecture when they are packaged into virions.

#### 4. Discussion and conclusions

Structural studies in the past ten years have led to a greatly improved understanding of -ssRNA virus-encoded NPs (Sun

et al., 2012). Although these NPs vary widely, their structures can be divided into two topological groups. The first group includes the majority of -ssRNA viral NPs, including BDV from the Bornaviridae family (Rudolph et al., 2003), VSV and rabies virus from the Phabdoviridae family (Albertini et al., 2006; Green et al., 2006), RSV from the Paramyxoviridae family (Tawar et al., 2009), influenza virus from the Orthomyxoviridae family (Ye et al., 2006), RVFV (Phlebovirus genus) (Raymond et al., 2010), and BUNV (Orthobunyavirus genus) (Li et al., 2013a) within the Bunyaviridae family. Although their detailed structures differ, NPs in class I generally have N- and C-lobes that face each other to form a positively charged crevice for RNA binding but use diverse structural components for inter-protomer interactions (Sun et al., 2012). NPs in class II include Lassa Fever virus (LASV, Arenaviridae family) (Hastie et al., 2011a,b; Qi et al., 2011) and CCHFV (Nairovirus genus, Bunyaviridae family) (Guo et al., 2012). Although LASV and CCHFV belong to different virus families and their NPs possess additional biological functions, the portions of their structures that carry out genome encapsidation share extremely high structural similarity.

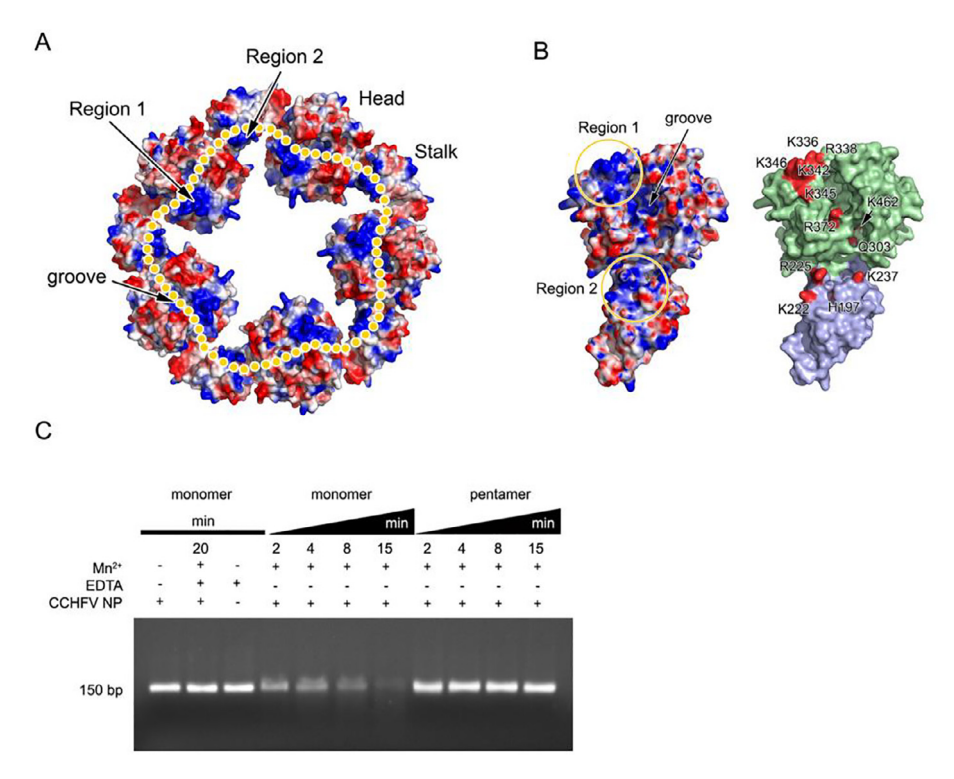


**Fig. 4.** RNA encapsidation channel in the CCHFV NP pentamer. (A) The electric potential surface of the CCHFV NP pentamer. Two regions located at the head and stalk domains and the groove in the head domain are labeled. The consecutive channel for RNA binding is indicated with a dotted line. (B) Localization of the positively-charged residues for RNA binding in the CCHFV NP protomer. The CCHFV NP protomer is shown with its electric potential surface and its molecular surface. Regions 1 and 2, the groove in the head domain and key residues are labeled. (C) Time series of an *in vitro* DNA degradation assay. The reaction products derived from 0.1  $\mu$ M purified CCHFV NP monomer or pentamer with 1 mM Mn<sup>2+</sup> and 100 ng/ $\mu$ l ssDNA as substrates at 16 °C in a final volume of 10  $\mu$ l, shown after 2, 4, 8, and 15 min. Reaction products were loaded onto a 20% polyacrylamide gel and stained with ethidium bromide.

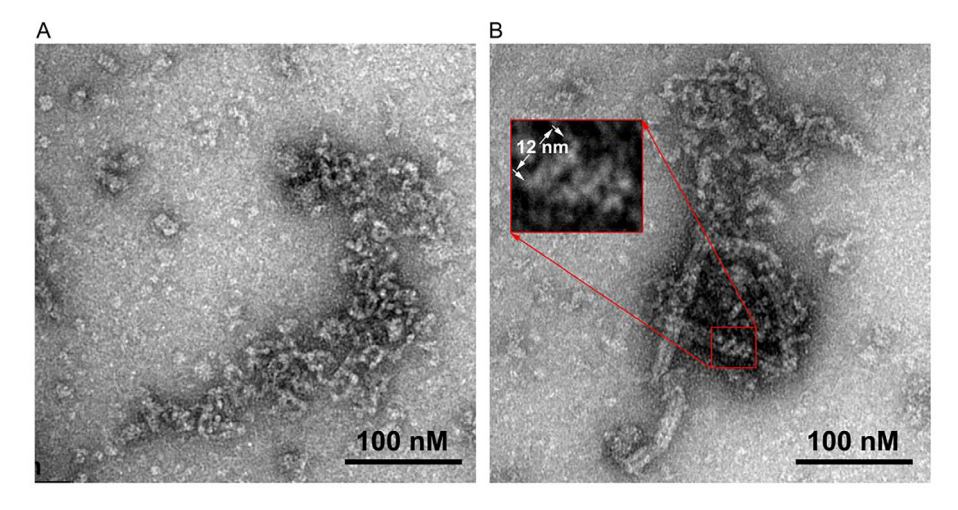
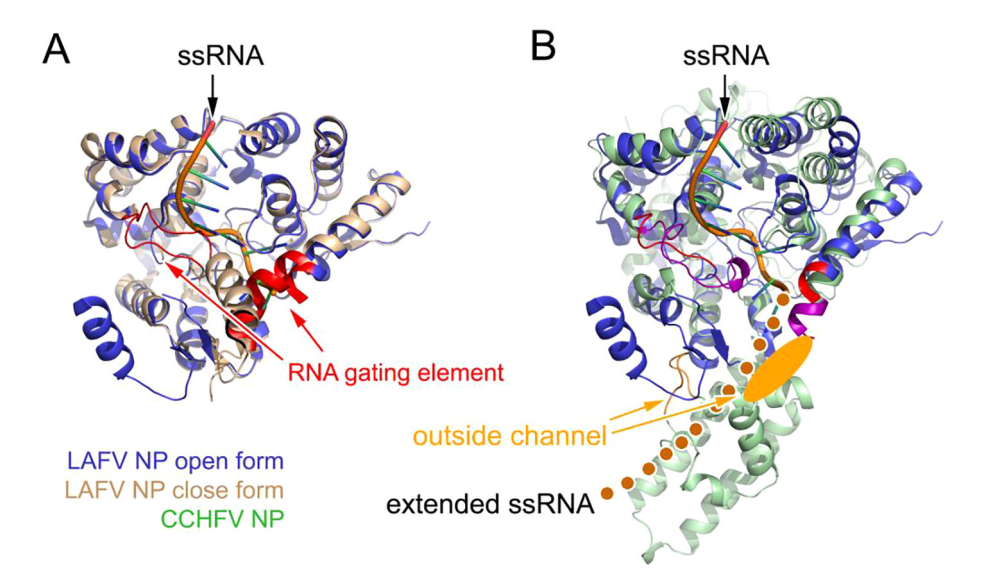


Fig. 5. EM image of native CCHFV RNPs extracted from CCHFV virions. (A) The majority of native CCHFV RNPs demonstrated flexible architecture with a width of approximately 5 nm. (B) In some images, native RNPs exhibited apparent helical characteristics with an approximate diameter of 12 nm (inset image).

The complex structure formed by the N-terminal domain of LASV NP and ssRNA revealed a novel RNA binding mode through a gating mechanism; this mechanism differs from that utilized by NPs in group I, which bind RNA in the crevice clamped by the N- and C-lobes (Hastie et al., 2011b). The structure of the CCHFV NP head domain presents high structural homology to the N-terminal domain of LASV NP, suggesting they may share a similar mechanism for RNA encapsidation. Comparison of the structure of CCHFV NP in its pentameric state and LASV with (PDB code: 3T5Q) (Hastie et al., 2011b) or without RNA (PDB code: 3MWT) (Qi et al., 2011) revealed a similar RNA gate with residues

D233-L239 in LASV NP and residues L362-M375 in CCHFV NP (Fig. 6). Although the structure of monomeric CCHFV NP was solved without RNA binding, the RNA gate in CCHFV NP presented a conformation similar to that in the RNA-containing LASV NP N-terminal domain (Fig. 6B). Moreover, in LASV NP,  $\alpha$ 5 was extended across the RNA binding pocket, and  $\alpha$ 6 was positioned on top of the pocket, preventing RNA from binding; however, residues K112-A122 of  $\alpha$ 5 became disordered, and  $\alpha$ 6 shifted away from the pocket to accommodate the RNA (Fig. 6A). In contrast, the corresponding region in CCHFV NP, i.e. M182-V193, existed in a disordered state, even without RNA binding. Interestingly, these



**Fig. 6.** A modified gating mechanism for RNA encapsidation of CCHFV NP. (A) Comparison of RNA-bound (PDB code: 3T5Q (Hastie et al., 2011b)) and RNA-free (PDB code: 3MWT (Qi et al., 2011)) structures of the N-terminal domain of LASV NP. Polypeptides of LASV NP with or without RNA are colored in blue and tan, respectively. The structural elements for the RNA gating mechanism, including the regions covering residues D233 to L239 and residues K112 to A122, are shown in red. Bound RNA is shown based on the coordination of 3T5Q. (B) Comparison of the RNA-bound (PDB code: 3T5Q (Hastie et al., 2011b)) LASV NP N-terminal domain and the monomeric structure of CCHFV NP in its pentameric state. LASV NP and CCHFV NP polypeptides are colored in blue and pale green, respectively. Bound RNA is shown based on the coordination of 3T5Q. Structural elements in CCHFV NP corresponding to the RNA gating element in LASV NP are colored in purple. The additional channel for CCHFV NP RNA binding is colored in gold, while the missing residues M182 to V193 are shown as ribbon diagrams.

two regions face each other and are located immediately downstream of the RNA-binding crevice in the CCHFV NP head domain, suggesting an additional RNA channel to accommodate the extended RNA from the RNA-binding crevice (Fig. 6B). Based on the RNA sequencing results, each CCHFV NP protomer binds 13–15 bases of RNA, but only 8 nt fit into the RNA-binding crevice in the head domain; thus, other structural portion(s) of CCHFV NP likely contribute to RNA encapsidation. A detailed crystal structure of the CCHFV NP-RNA oligomer at the atomic level is required to finalize this model.

Notably, the RNA binding groove overlaps with the active site of the CCHFV NP endonuclease in this model. Monomeric CCHFV NP exhibits DNA-specific endonuclease activity for which the residues in the groove of the head domain are essential (Guo et al., 2012), but this endonuclease activity was abrogated by RNA binding (Fig. 4C). We thus hypothesize that the enzymatic activity of CCHFV NP is inhibited in an RNP state, but monomeric CCHFV NP, which exists in a free state, is either newly translated or released from RNP during genome replication, contributing to other steps of the viral life cycle. Elucidation of the precise role of this unusual activity requires further biological evidence.

The mechanism underlying viral NP recognition of genomic RNA to initiate RNA encapsidation also requires investigation. Certain special sequences or stem-loop structures in the 5' or 3' end of the viral genome act as packaging signals for NP recognition and RNP formation (Mir and Panganiban, 2004, 2005; Mir et al., 2006; Sun et al., 2014). However, structural studies of the viral NP-RNA complex have not elucidated the specificity of NP-RNA recognition. RNAs extracted from the recombinant NP-RNA complex formed during protein expression demonstrate no sequence or structural features (Albertini et al., 2006; Green et al., 2006; Hastie et al., 2011b; Li et al., 2013a; Mohl and Barr, 2009; Niu et al., 2013; Tawar et al., 2009). Reconstruction of the viral NP and nucleic acid complex is easily achieved by incubating viral NP with nucleic acids, RNA or even DNA, lacking any sequence or structural specificity (Jiao et al., 2013; Raymond et al., 2012). Furthermore, there is no evidence supporting a potential key structural element that specifically binds RNA. NP residues interact with the hydroxyl group of ribose in RNA in the RSV NP-RNA complex but do not support binding specificity (Tawar et al., 2009). Unlike other NPs in group I, CCHFV NP predominantly exists as a monomer under physiological conditions and does not form an oligomer if additional random nucleic acids are supplied (Guo et al., 2012), suggesting a high specificity for RNA possessing sequence or structural specificity. We first identified the existence of the CCHFV NP-RNA complex and isolated it from a large volume of expression cells. Sequencing of the RNAs extracted from naturally formed NP-RNA complexes revealed sequence similarities between the bound RNAs and the sequences of the 5' and 3' ends of the CCHFV S segment, suggesting a potential packaging signal for the initiation of genome encapsidation. We are still working to verify this hypothesis. If confirmed, CCHFV will be a good model to investigate the specificity of viral NP-RNA recognition. Similar observations were made for LASV NP oligomerization (Brunotte et al., 2011: Hastie et al., 2011b: Oi et al., 2011), Although LASV NP exhibited a ring-shaped structure, as visualized using EM or small-angle X-ray scattering, no RNA was observed in the crystal structure, and the crystallographic symmetry of the LASV NP trimer suggested the participation of C-terminal exonuclease activity in genome encapsidation (Brunotte et al., 2011; Hastie et al., 2011b; Qi et al., 2011). Therefore, the specificity for RNA binding and further interpretation of the role of the LASV NP C-terminal domain in RNA binding require further elucidation.

The formation of –ssRNA viral RNP is much more complicated than indicated either by crystal structures or EM mapping and is likely highly dependent on the conditions under which the RNP exists, or even the purification conditions. For example, the coexistence of tetrameric, pentameric, and hexameric ring-shaped architectures complexes has been characterized for recombinant phlebovirus and orthobunyavirus NP-RNA complexes, but EM visualization of natural RNPs extracted from RVFV and BUNV virions suggests a flexible organization in which a monomer-sized NP-RNA complex is likely the building block of these chain-like RNPs (Ariza et al., 2013; Dong et al., 2013a; Ferron et al., 2011; Jiao

et al., 2013; Li et al., 2013a; Niu et al., 2013; Olal et al., 2014; Raymond et al., 2012; Reguera et al., 2013; Zhou et al., 2013b). In contrast, Ariza et al. observed a well-defined helical architecture for extracted natural BUNV RNP, suggesting a tetrameric building block, which was also observed in the crystal structure (Ariza et al., 2013). The analysis of natural LACV RNPs has produced combined results, in which the majority of RNPs are present with a flexible architecture but some of them form helical shapes with widths similar to the tetrameric structure obtained by crystallization (Reguera et al., 2013). The diversity of high-ordered natural RNP structures is likely attributable to the different conditions utilized for purification and EM negative staining. Similar to the variations present among high-ordered structures of phlebovirus and orthobunyavirus natural RNPs, we also observed the presence of tetrameric, pentameric, hexameric and heptameric CCHFV NP-RNA rings and the combination of flexible and helical structures in natural RNPs (Fig. 5: Supplementary Fig. S1). Although the pentamer form was the most abundant fraction among all of the multimers, the helical structure observed in EM images of natural CCHFV NPs suggested a width similar with the size of a tetrameric CCHFV NP-RNA complex (Fig. 5). Considering the limited space inside virions, we speculated that bunyaviruses, at least nairoviruses and orthobunyaviruses, form RNPs with high-ordered helical architecture in which the tetrameric NP-RNA complex represents the building block during the packaging of RNPs into virions. Two substantial breakthroughs regarding influenza virus RNP formation revealed large structural discrepancies between real or authentic viral RNPs and the proposed model based on crystal structures of NP proteins (Arranz et al., 2013; Moeller et al., 2013). Therefore, further work is required to investigate the structures of reconstructed authentic bunyaviral RNPs formed when L and NP are expressed together with transcribed viral RNA in mammalian cells and integrate these observations.

#### Acknowledgments

This work was supported by the National Natural Science Foundation of China (Grant no. 81322023, 31370733, 31300606, 31170678 and 31100208), the 973 program of Ministry of Science and Technology (Grant No. 2013CB911100 and 2014CB542800), and Tsinghua University Initiative Scientific Research Program (2009THZ01).

#### Appendix A. Supplementary data

Supplementary data associated with this article can be found, in the online version, at http://dx.doi.org/10.1016/j.jsb.2016.09.013.

#### References

- Albertini, A.A., Wernimont, A.K., Muziol, T., Ravelli, R.B., Clapier, C.R., Schoehn, G., Weissenhorn, W., Ruigrok, R.W., 2006. Crystal structure of the rabies virus nucleoprotein-RNA complex. Science 313, 360–363.
- Ariza, A., Tanner, S.J., Walter, C.T., Dent, K.C., Shepherd, D.A., Wu, W., Matthews, S.V., Hiscox, J.A., Green, T.J., Luo, M., Elliott, R.M., Fooks, A.R., Ashcroft, A.E., Stonehouse, N.J., Ranson, N.A., Barr, J.N., Edwards, T.A., 2013. Nucleocapsid protein structures from orthobunyaviruses reveal insight into ribonucleoprotein architecture and RNA polymerization. Nucl. Acids Res. 41, 5912–5926.
- Arranz, R., Coloma, R., Chichon, F.J., Conesa, J.J., Carrascosa, J.L., Valpuesta, J.M., Ortin, J., Martin-Benito, J., 2013. The structure of native influenza virion ribonucleoproteins. Science 338, 1634–1637.
- Arstila, P., 1974. Characteristics of vesicular stomatitis virus envelopes released with saponin. J. Gen. Virol. 24, 319–326.
- Bergeron, E., Albarino, C.G., Khristova, M.L., Nichol, S.T., 2012. Crimean-Congo hemorrhagic fever virus-encoded ovarian tumor protease activity is dispensable for virus RNA polymerase function. J. Virol. 84, 216–226.
- Brunotte, L., Kerber, R., Shang, W., Hauer, F., Hass, M., Gabriel, M., Lelke, M., Busch, C., Stark, H., Svergun, D.I., Betzel, C., Perbandt, M., Gunther, S., 2011. Structure of

- the Lassa virus nucleoprotein revealed by X-ray crystallography, small-angle X-ray scattering, and electron microscopy. J. Biol. Chem. 286, 38748–38756.
- Carter, S.D., Surtees, R., Walter, C.T., Ariza, A., Bergeron, E., Nichol, S.T., Hiscox, J.A., Edwards, T.A., Barr, J.N., 2012. Structure, function, and evolution of the Crimean-Congo hemorrhagic Fever virus nucleocapsid protein. J. Virol. 86, 10914–10923.
- Dong, H., Li, P., Elliott, R.M., Dong, C., 2013a. Structure of Schmallenberg orthobunyavirus nucleoprotein suggests a novel mechanism for genome encapsidation. J. Virol. 87, 5593–5601.
- Dong, H., Li, P., Bottcher, B., Elliott, R.M., Dong, C., 2013b. Crystal structure of Schmallenberg orthobunyavirus nucleoprotein-RNA complex reveals a novel RNA sequestration mechanism. RNA 19, 1129–1136.
- Eifan, S.A., Elliott, R.M., 2009. Mutational analysis of the Bunyamwera orthobunyavirus nucleocapsid protein gene. J. Virol. 83, 11307–11317.
- Elliott, R.M., 1990. Molecular biology of the Bunyaviridae. J. Gen. Virol. 71, 501–522. Elliott, R.M., 2014. Orthobunyaviruses: recent genetic and structural insights. Nat. Rev. Microbiol. 12, 673–685.
- Emsley, P., Lohkamp, B., Scott, W.G., Cowtan, K., 2010. Features and development of Coot. Acta Crystallogr. A 66, 486–501.
- Ferron, F., Li, Z., Danek, E.I., Luo, D., Wong, Y., Coutard, B., Lantez, V., Charrel, R., Canard, B., Walz, T., Lescar, J., 2011. The hexamer structure of Rift Valley fever virus nucleoprotein suggests a mechanism for its assembly into ribonucleoprotein complexes. PLoS Pathog. 7, e1002030.
- Flick, R., Whitehouse, C.A., 2005. Crimean-Congo hemorrhagic fever virus. Curr. Mol. Med. 5, 753–760.
- Green, T.J., Zhang, X., Wertz, G.W., Luo, M., 2006. Structure of the vesicular stomatitis virus nucleoprotein-RNA complex. Science 313, 357–360.
- Guo, Y., Wang, W., Ji, W., Deng, M., Sun, Y., Zhou, H., Yang, C., Deng, F., Wang, H., Hu, Z., Lou, Z., Rao, Z., 2012. Crimean-Congo hemorrhagic fever virus nucleoprotein reveals endonuclease activity in bunyaviruses. Proc. Natl. Acad. Sci. U.S.A. 109, 5046–5051.
- Guo, X., Brenner, M., Zhang, X., Laragione, T., Tai, S., Li, Y., Bu, J., Yin, Y., Shah, A.A., Kwan, K., Li, Y., Jun, W., Gulko, P.S., 2013. Whole-genome sequences of DA and F344 rats with different susceptibilities to arthritis, autoimmunity, inflammation and cancer. Genetics 194, 1017–1028.
- Guu, T.S., Zheng, W., Tao, Y.J., 2012. Bunyavirus: structure and replication. Adv. Exp. Med. Biol. 726, 245–266.
- Hastie, K.M., Kimberlin, C.R., Zandonatti, M.A., MacRae, I.J., Saphire, E.O., 2011a. Structure of the Lassa virus nucleoprotein reveals a dsRNA-specific 3' to 5' exonuclease activity essential for immune suppression. Proc. Natl. Acad. Sci. U.S. A. 108, 2396–2401.
- Hastie, K.M., Liu, T., Li, S., King, L.B., Ngo, N., Zandonatti, M.A., Woods Jr., V.L., de la Torre, J.C., Saphire, E.O., 2011b. Crystal structure of the Lassa virus nucleoprotein-RNA complex reveals a gating mechanism for RNA binding. Proc. Natl. Acad. Sci. U.S.A. 108, 19365–19370.
- Jiao, Y., Zeng, X., Guo, X., Qi, X., Zhang, X., Shi, Z., Zhou, M., Bao, C., Zhang, W., Xu, Y., Wang, H., 2011. Preparation and evaluation of recombinant severe fever with thrombocytopenia syndrome virus nucleocapsid protein for detection of total antibodies in human and animal sera by double-antigen sandwich enzymelinked immunosorbent assay. J. Clin. Microbiol. 50, 372–377.
- Jiao, L., Ouyang, S., Liang, M., Niu, F., Shaw, N., Wu, W., Ding, W., Jin, C., Peng, Y., Zhu, Y., Zhang, F., Wang, T., Li, C., Zuo, X., Luan, C.H., Li, D., Liu, Z.J., 2013. Structure of severe fever with thrombocytopenia syndrome virus nucleocapsid protein in complex with suramin reveals therapeutic potentials. I. Virol. 87. 6829–6839.
- Karlberg, H., Tan, Y.J., Mirazimi, A., 2011. Induction of caspase activation and cleavage of the viral nucleocapsid protein in different cell types during Crimean-Congo hemorrhagic fever virus infection. J. Biol. Chem. 286, 3227– 3234.
- Kouprina, N., Larionov, V., 2008. Selective isolation of genomic loci from complex genomes by transformation-associated recombination cloning in the yeast Saccharomyces cerevisiae. Nat. Protoc. 3, 371–377.
- Li, B., Wang, Q., Pan, X., Fernandez de Castro, I., Sun, Y., Guo, Y., Tao, X., Risco, C., Sui, S.F., Lou, Z., 2013a. Bunyamwera virus possesses a distinct nucleocapsid protein to facilitate genome encapsidation. Proc. Natl. Acad. Sci. U.S.A. 110, 9048–9053.
- Li, K., Yang, Q., Wang, W., Zhao, X., Lou, Z., 2013b. GPX3 from Arabidopsis thaliana: cloning, expression, purification, crystallization and preliminary X-ray analysis. Acta Crystallogr., Sect. F: Struct. Biol. Cryst. Commun. 69, 1224–1226.
- Li, X., Mooney, P., Zheng, S., Booth, C.R., Braunfeld, M.B., Gubbens, S., Agard, D.A., Cheng, Y., 2013c. Electron counting and beam-induced motion correction enable near-atomic-resolution single-particle cryo-EM. Nat. Methods 10, 178– 180.
- Lou, Z., Sun, Y., Rao, Z., 2014. Current progress in antiviral strategies. Trends Pharmacol. Sci. 35, 86–102.
- Mindell, J.A., Grigorieff, N., Mindell, J.A., Grigorieff, N., 2003. Accurate determination of local defocus and specimen tilt in electron microscopy. J. Struct. Biol. 142, 334–347.
- Mir, M.A., Panganiban, A.T., 2004. Trimeric hantavirus nucleocapsid protein binds specifically to the viral RNA panhandle. J. Virol. 78, 8281–8288.
- Mir, M.A., Panganiban, A.T., 2005. The hantavirus nucleocapsid protein recognizes specific features of the viral RNA panhandle and is altered in conformation upon RNA binding. J. Virol. 79, 1824–1835.
- Mir, M.A., Brown, B., Hjelle, B., Duran, W.A., Panganiban, A.T., 2006. Hantavirus N protein exhibits genus-specific recognition of the viral RNA panhandle. J. Virol. 80, 11283–11292.
- Moeller, A., Kirchdoerfer, R.N., Potter, C.S., Carragher, B., Wilson, I.A., 2013.
  Organization of the influenza virus replication machinery. Science 338, 1631–
  1634

- Mohl, B.P., Barr, J.N., 2009. Investigating the specificity and stoichiometry of RNA binding by the nucleocapsid protein of Bunyamwera virus. RNA 15, 391–399.
- Niu, F., Shaw, N., Wang, Y.E., Jiao, L., Ding, W., Li, X., Zhu, P., Upur, H., Ouyang, S., Cheng, G., Liu, Z.J., 2013. Structure of the Leanyer orthobunyavirus nucleoprotein-RNA complex reveals unique architecture for RNA encapsidation. Proc. Natl. Acad. Sci. U.S.A. 110, 9054–9059.
- Olal, D., Dick, A., Woods Jr., V.L., Liu, T., Li, S., Devignot, S., Weber, F., Saphire, E.O., Daumke, O., 2014. Structural insights into RNA encapsidation and helical assembly of the Toscana virus nucleoprotein. Nucleic Acids Res. 42, 6025–6037.
- Osborne, J.C., Elliott, R.M., 2000. RNA binding properties of bunyamwera virus nucleocapsid protein and selective binding to an element in the 5' terminus of the negative-sense S segment. J. Virol. 74, 9946–9952.
- Pettersen, E.F., Goddard, T.D., Huang, C.C., Couch, G.S., Greenblatt, D.M., Meng, E.C., Ferrin, T.E., 2004. UCSF Chimera–a visualization system for exploratory research and analysis. J. Comput. Chem. 25, 1605–1612.
- Qi, X., Lan, S., Wang, W., Schelde, L.M., Dong, H., Wallat, G.D., Ly, H., Liang, Y., Dong, C., 2011. Cap binding and immune evasion revealed by Lassa nucleoprotein structure. Nature 468, 779–783.
- Qing, J., Wang, Y., Sun, Y., Huang, J., Yan, W., Wang, J., Su, D., Ni, C., Li, J., Rao, Z., Liu, L., Lou, Z., 2014. Cyclophilin a associates with enterovirus-71 virus capsid and plays an essential role in viral infection as an uncoating regulator. PLoS Pathog. 10, e1004422.
- Raymond, D.D., Piper, M.E., Gerrard, S.R., Smith, J.L., 2010. Structure of the Rift Valley fever virus nucleocapsid protein reveals another architecture for RNA encapsidation. Proc. Natl. Acad. Sci. U.S.A. 107, 11769–11774.
- Raymond, D.D., Piper, M.E., Gerrard, S.R., Skiniotis, G., Smith, J.L., 2012. Phleboviruses encapsidate their genomes by sequestering RNA bases. Proc. Natl. Acad. Sci. U.S.A. 109, 19208–19213.
- Reguera, J., Malet, H., Weber, H., Cusack, S., 2013. Structural basis for encapsidation of genomic RNA by La Crosse Orthobunyavirus nucleoprotein. Proc. Natl. Acad. Sci. U.S.A. 110, 7246–7251.

- Rudolph, M.G., Kraus, I., Dickmanns, A., Eickmann, M., Garten, W., Ficner, R., 2003. Crystal structure of the borna disease virus nucleoprotein. Structure 11, 1219–1226.
- Ruigrok, R.W., Crepin, T., Kolakofsky, D., 2011. Nucleoproteins and nucleocapsids of negative-strand RNA viruses. Curr. Opin. Microbiol. 14, 504–510.
- Scheres, S.H., 2012. RELION: implementation of a Bayesian approach to cryo-EM structure determination. J. Struct. Biol. 180, 519–530.
- Scheres, S.H., Chen, S., 2012. Prevention of overfitting in cryo-EM structure determination. Nat. Methods 9, 853–854.
- Sun, Y., Guo, Y., Lou, Z., 2012. A versatile building block: the structures and functions of negative-sense single-stranded RNA virus nucleocapsid proteins. Protein Cell 3, 893–902.
- Sun, Y., Guo, Y., Lou, Z., 2014. Formation and working mechanism of the picornavirus VPg uridylylation complex. Curr. Opin. Virol. 9C, 24–30.
- Tawar, R.G., Duquerroy, S., Vonrhein, C., Varela, P.F., Damier-Piolle, L., Castagne, N., MacLellan, K., Bedouelle, H., Bricogne, G., Bhella, D., Eleouet, J.F., Rey, F.A., 2009. Crystal structure of a nucleocapsid-like nucleoprotein-RNA complex of respiratory syncytial virus. Science 326, 1279-1283.
- Wang, Y., Dutta, S., Karlberg, H., Devignot, S., Weber, F., Hao, Q., Tan, Y.J., Mirazimi, A., Kotaka, M., 2012. Structure of Crimean-Congo hemorrhagic fever virus nucleoprotein: superhelical homo-oligomers and the role of caspase-3 cleavage. J. Virol. 86, 12294–12303.
- Ye, Q., Krug, R.M., Tao, Y.J., 2006. The mechanism by which influenza a virus nucleoprotein forms oligomers and binds RNA. Nature 444, 1078–1082.
- Zhou, H., Sun, Y., Guo, Y., Lou, Z., 2013a. Structural perspective on the formation of ribonucleoprotein complex in negative-sense single-stranded RNA viruses. Trends Microbiol. 21, 475–484.
- Zhou, H., Sun, Y., Liu, M., Wang, Y., Liu, C., Wang, W., Liu, X., Li, L., Deng, F., Guo, Y., Lou, Z., 2013b. The nucleoprotein of severe fever with thrombocytopenia syndrome virus processes an oligomeric ring to facilitate RNA encapsidation. Protein Cell 4, 445–455.